Anisotropic Outputs of a Nanogenerator from Oblique-Aligned ZnO Nanowire Arrays

Cheng-Ying Chen,[†,‡] Jun-Han Huang,[§,∥,∞] Jinhui Song,[‡] Yusheng Zhou,[‡] Long Lin,[‡] Po-Chien Huang,[§] Yan Zhang,[‡,⊥] Chuan-Pu Liu,[§,∥,∞] Jr-Hau He,[†,*] and Zhong Lin Wang[‡,*]

[†]Institute of Photonics and Optoelectronics and Department of Electrical Engineering, National Taiwan University, Taipei, 10617 Taiwan, [‡]School of Materials Science and Engineering, Georgia Institute of Technology, Atlanta, Georgia 30332-0245, United States, [§]Department of Materials Science and Engineering, [∥]Research Center for Energy Technology and Strategy, [∞]Center for Micro/Nano Science and Technology, National Cheng Kung University, Tainan, 701 Taiwan, and [⊥]Institute of Theoretical Physics, Lanzhou University, Lanzhou, Gansu 73000, People's Republic of China

ABSTRACT We studied the dependence of the output of the piezoelectric nanogenerator (NG) on the inclining orientation of the ZnO nanowire arrays (NWAs). The oblique-aligned NWAs were grown by combing a modified oblique-angle sputtering technique for preparing the seed layer and hydrothermal growth. The piezoelectric output of the NWAs was studied by scanning the tip of an atomic force microscope along four different directions in reference to the inclining direction of the NWs. The statistical outputs were analyzed in reference to the theoretically calculated piezopotential distribution in the NWs. Our study provides in-depth understanding about the performance of NGs.

KEYWORDS: ZnO · nanowire · atomic force microscope · nanogenerator

Renewable energy plays a crucial role in the sustainable development of human civilization.[1−3] In nanotechnology, it is a key challenge to find a power source that can drive the nanodevices without adding much volume. Mechanical energy, such as body movement, vibration of acoustic waves, light wind, hydraulic energy, and heart beating, has been proposed as a potential energy source for powering small electronic components, including implantable biosensors, microelectromechanical systems, nanorobots, and even portable personal electronics.[4] As for these applications, great progress has been made in developing piezoelectric nanogenerators (NGs) based on ZnO nanowires (NWs)/nanotubes,[5−9] CdS NWs,[10] ZnS NWs,[11] PZT nanofibers/ribbons,[12,13] $BaTiO_3$,[14] polyvinylidene fluoride,[15] InN NWs,[16] AlGaN nanocones,[17] and GaN nanorods.[17−19]

Among these piezoelectric materials, ZnO is one of the most promising materials due to the following three key advantages. First, ZnO is biocompatible, degradable, and nontoxic.[20] Second, ZnO is easy to synthesize and is low-cost. Third, ZnO nanostructures are also recognized as the potential material for optoelectronic/sensor nanodevices, such as light emitting diodes,[21,22] photodetectors,[23−27] and gas/chemical sensors.[27,28] Therefore, ZnO nanostructures as the NG materials can be beneficial to the integration of various ZnO-based self-power nanodevices.

The current study has been mainly focused on vertically aligned ZnO NW arrays. In this paper, we study the effect of NW orientation on the NG output experimentally and theoretically. A combined method of modified oblique-angle deposition (OAD) and hydrothermal growth was utilized to obtain the oblique-aligned ZnO NW arrays (NWAs). Due to the reduction of the in-plane symmetry in the NWAs, the output of the NG depends on the direction along which the tip of the atomic force microscope (AFM) scans. The anisotropic electricity generation was statistically demonstrated and analyzed on the oblique-aligned ZnO NWAs with four different scanning directions. Furthermore, the ZnO NWAs also show excellent NG performance due to the highly conductive Al-doped ZnO (AZO) buffer layer as the bottom electric contact. Our study provides the guidance for optimizing the output of NGs.

RESULTS AND DISCUSSION

The oblique-aligned ZnO NWAs were synthesized by combining the oblique-angle sputtering in the reductive atmosphere and the hydrothermal growth. The detailed growth method is given in Experimental Section. Figure 1a shows the cross-sectional scanning electron microscopy (SEM) image of the oblique-aligned ZnO NWAs. The diameter and the length of the NWs are ∼50 nm and ∼1 μm, respectively. The tilted angles of the NWs are around 20° relative to substrate normal. The OAD leads to the

* Address correspondence to zlwang@gatech.edu, jhhe@cc.ee.ntu.edu.tw.

Received for review June 18, 2011 and accepted July 20, 2011.

Published online July 20, 2011
10.1021/nn202251m

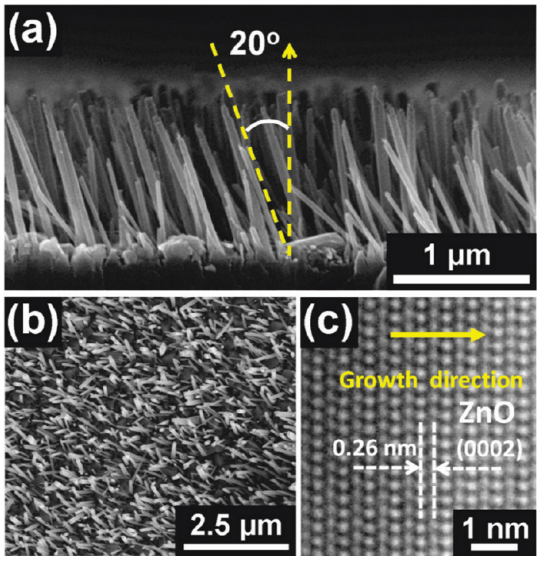

Figure 1. (a) Cross-sectional and (b) top-view SEM image of the oblique-aligned ZnO NWAs. (c) HRTEM image of a ZnO NW.

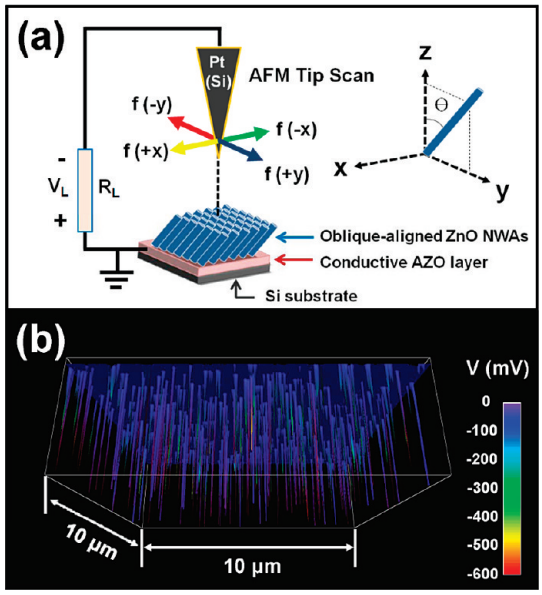

Figure 2. Piezoelectric power generation using the n-type oblique-aligned ZnO NWAs. (a) Schematic of the AFM measurement system with four different scanning directions of the AFM tip [*f* (+*x*), *f* (−*x*), *f* (+*y*), and *f* (−*y*)], and schematic of the oblique-aligned ZnO NWAs. Coordinate system is used to define the direction of lateral force applied from the AFM tip. (Note that the defined polarity of the output voltage signal is V_L.) (b) Three-dimensional plot of the output voltage (along −*x*-axis direction) at an external load (R_L = 500 MΩ) recorded when the AFM tip is scanned across the NWAs with an area of 10 μm × 10 μm.

formation of a bent columnar ZnO seed layer (at the top of the AZO buffer layer) inclined from the substrate normal in the opposite direction to the incident vapor beam owing to surface-diffusion-enhanced self-shadowing effect.[29] The oblique-aligned ZnO NWAs were uniformly synthesized on the bent columnar ZnO seed layers using a solution method, as shown in Figure 1b. The seeded layer is oriented with its bent *c*-axis along the opposite direction of sputtering and the NWs grown along the *c*-axis of ZnO, resulting in the formation of the declined arrays.[29] A high-resolution transmission electron microscopy (HRTEM) image indicates that the NWs are single crystalline, as shown in Figure 1c. The measured interplanar distance of 0.26 nm corresponds to the ZnO(0002) planes, showing that the NWs grow preferentially along the *c*-axis direction (*i.e.*, [0001]).

The piezoelectric responses of the oblique-aligned ZnO NWAs were examined using AFM in contact mode with four different scanning directions of a Pt-coated Si tip, as shown in Figure 2a. Figure 2b exhibits the three-dimensional (3D) distribution of output potential generated by the ZnO NWAs with a scanning area of 10 μm × 10 μm, and the color code represents the magnitude of the output potential. The AFM tip scans across the sample to laterally bend the ZnO NWAs, and the output electrical signals are consecutively monitored and recorded across an external load (R_L = 500 MΩ). According to Kirchhoff's voltage law, it has been noticed that the measured voltage signals are always much lower than the calculated ones, which is likely due to significant contact resistance between Ag pastes and thin films at the bottom of the NWs, resistance of the bottom thin film, contact resistance between the Pt tip and the NWs, limited conductivity, and small capacitance of the NWs.[3,17,30,31] To increase the measured voltage signals in the oblique-aligned ZnO NWAs, the highly conductive Al-doped ZnO (AZO) buffer layer (resistiviy, $\rho = 1.29 \times 10^{-4}$ Ωcm determined by four-point probe measurements) was utilized as the bottom electric contact instead of the intrinsic ZnO layer ($\rho \sim 0.55$ Ωcm).[5,6] The internal resistance of our oblique-aligned ZnO NWAs based the NG is around 25 MΩ. The detailed growth of the AZO buffer layer can be seen in the Experimental Section. Furthermore, as shown in Figure 2b, negative sharp output voltage peaks result from the piezoelectric potential-driven transient flow of electrons across the load as the tip consecutively scanned across the NWAs. Some output signals could reach several hundred negative millivolts, which is much higher than those received (around −6 to −35 mV) for the ZnO NWAs with the intrinsic ZnO layer as a bottom electric contact.[5,32] Moreover, the average output voltages (around −130 to −160 mV), as shown in Figure 3, are also higher than these of high-output NGs based on the InN and GaN NWAs,[16,19] which ascribes to the highly conductive AZO buffer layer as the bottom electric contact.

Due to the reduction of the in-plane symmetry in the NWAs, the anisotropic electricity generation is expected on the oblique-aligned ZnO NWAs with different scanning directions of the AFM tip. To distinguish the anisotropy of electricity generation based on the

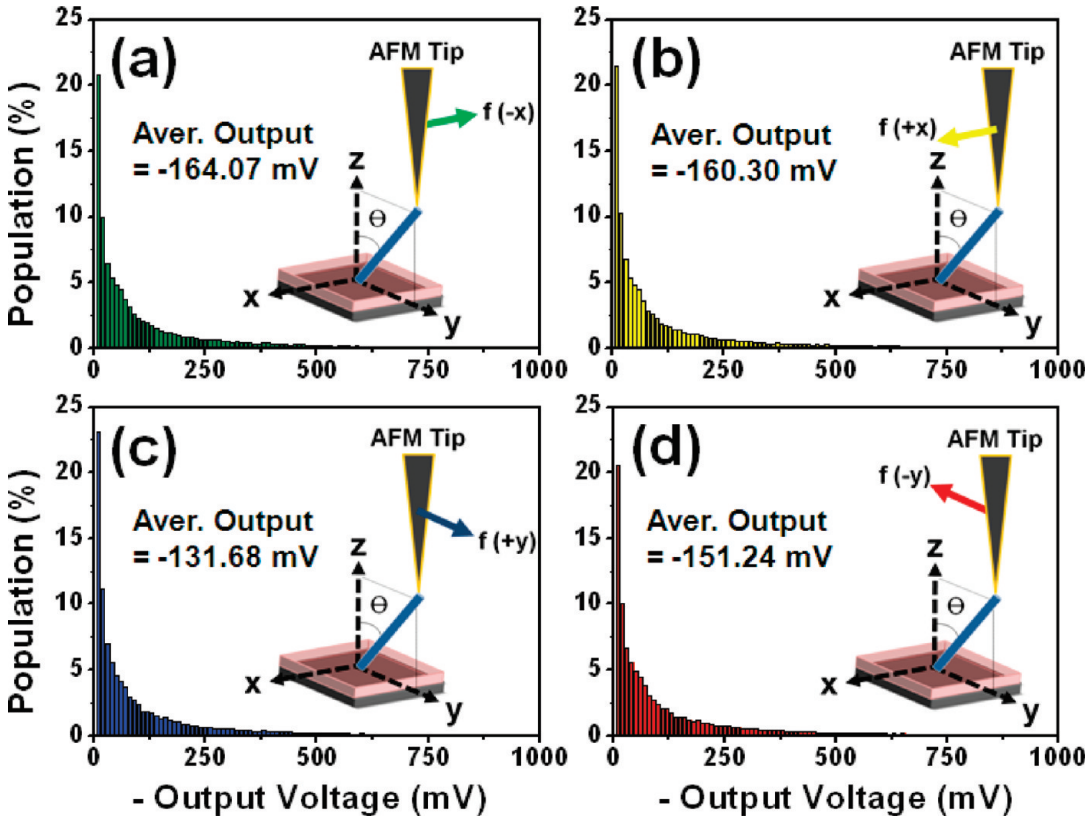

Figure 3. Statistical distribution of the piezoelectric output measured from the oblique-aligned ZnO NWAs with the AFM tip scanning along (a) $-x$-axis direction (the amount of statistical peaks = 44 830), (b) $+x$-axis direction (the amount of statistical peaks = 44 533), (c) $+y$-axis direction (the amount of statistical peaks = 34 525), and (d) $-y$-axis direction (the amount of statistical peaks = 36 333).

oblique-aligned ZnO NWAs, we plotted the statistical distribution of the measured piezoelectric output with the AFM tip scanning along $\pm x$-axis and $\pm y$-axis directions, as shown in Figure 3. The amount of statistical peaks for each scanning direction is larger than 34 000 peaks, which were measured at the different areas of 10 μm $\times$ 10 μm. Because the areas used for each measurement are different, density, morphology, tilted angle, and aspect ratio of oblique-aligned ZnO NWAs are varied slightly. Therefore, the measured piezoelectric output with each tip scanning exhibits statistical distributions: about 55−60% of output voltages are within the range from −2 to −100 mV; about 20−30% of output voltages are within the range from −100 to −200 mV, and some output voltages could reach several hundred negative millivolts. Moreover, one can see that the average piezoelectric voltages along $\pm x$-axis directions are almost identical (around −160 mV) (Figure 3a, b) and are higher than those along $+y$-axis direction (around −130 mV in Figure 3c) and $-y$-axis direction (around −150 mV in Figure 3d). The output difference between $+y$-axis and $-y$-axis directions could be up to around 20 mV, which is comparable to the piezoelectric output of the previous ZnO NGs.[5,32] Accordingly, significant anisotropy of electricity generation was demonstrated on the oblique-aligned ZnO NWAs.

To understand the mechanism of the anisotropic electricity generation based on the oblique-aligned ZnO NWAs, the piezopotential distribution in a bent inclined ZnO NW was calculated under a lateral force (f) with different directions. Although the magnitude of the piezopotential is significantly related to the carrier concentration and their distribution,[31,33] a semiquantitative understanding can be achieved by numerical calculation without considering the carrier concentration. For simplicity, we assume that an oblique NW is fixed at one end (bottom side) and the other end is pushed by a point force analogous to the scanning action of an AFM tip, as shown in Figure 4a. Note that for applied force f, the effective force for bending the NW along $\pm x$-axis directions is f (Figure 4b) while the effective force along $\pm y$-axis directions is $f \cdot \cos\theta$ (Figure 4c,d). For the applied lateral force f along $\pm y$-axis directions, as we neglect the slip between an AFM tip and the NW, the partial forces $f \cdot \sin\theta$ along $\pm c$-axis directions apply on the inclined NW, as shown in Figure 4c,d. Furthermore, the Lippman theory was utilized to calculate the piezopotential distribution in a bent ZnO NW.[31] The material constants used in the calculation includ the following: anisotropic elastic constants of ZnO: C_{11} = 207 GPa, C_{12} = 117.7 GPa, C_{13} = 106.1 GPa, C_{33} = 209.5 GPa, C_{44} = 44.8 GPa, C_{55} = 44.6

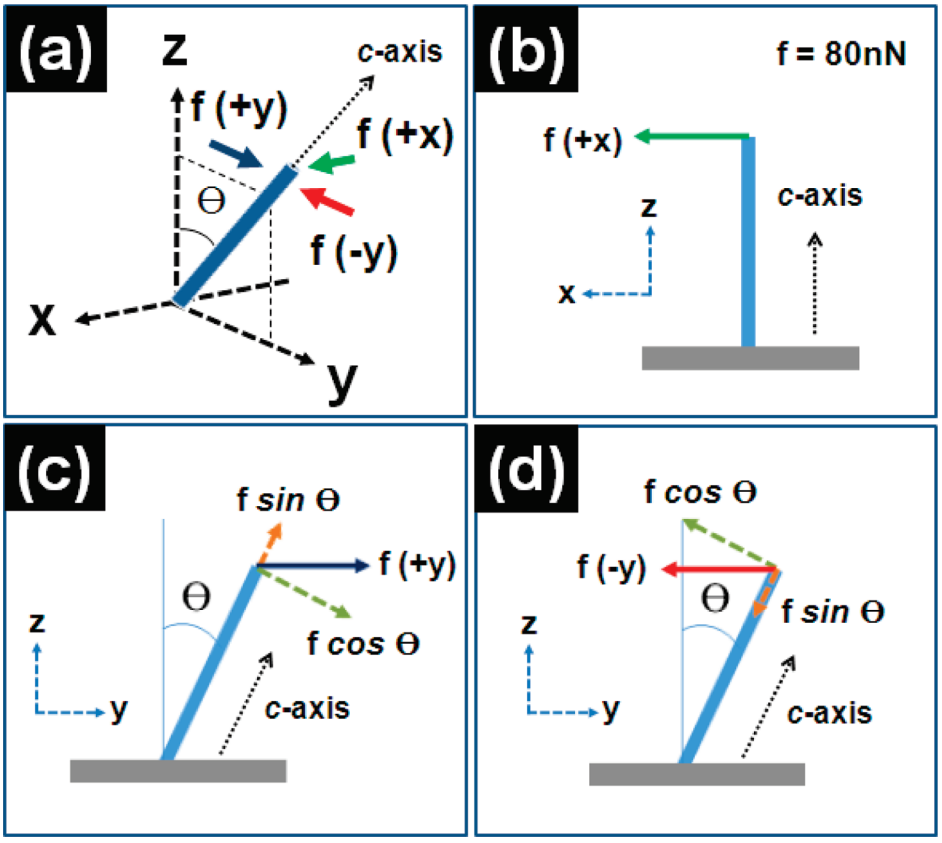

Figure 4. (a) Coordinate system is used to define the direction of lateral force applied from the AFM tip. The tilted angle is $\theta = 20°$; an AFM tip pushes the ZnO NW along (b) $+x$-axis direction, (c) $+y$-axis direction, and (d) $-y$-axis direction.

GPa; and piezoelectric constants: $e_{15} = -0.45$ C/m^2, $e_{31} = -0.51$ C/m^2, $e_{33} = 1.22$ C/m^2. The relative dielectric constants are $k_{\perp} = 7.77$, $k_{||} = 8.91$, and the density (ρ) is 5680 kg/m^3.[34] Length, diameter, and tilted angle of the ZnO NW with a growth direction of [0001] was set to be 1 μm, 50 nm, and 20°, respectively. The applied f was set to be 80 nN.[6]

The calculated piezopotential distributions in the bent ZnO NW are revealed and viewed from the side (Figure 5a–e) and the top (Figure 5f–j) of the NW. Figure 5a (side view) and 5f (top view) represent the calculated piezopotential distributions in the bent inclined ZnO NW pushed by an AFM tip along $+x$-axis direction (Figure 4b). According to our previous studies, positive potential and negative potential are created along the stretched side (the outer surface) and compressed side (the inner surface) of the NW, respectively.[5,6] When the tip scans across the top of the NW and touches the compressed side of the NW, the negative piezopotential sets the Schottky barrier (at the interface between the Pt-coated tip and the ZnO NW) to forward bias, thus the free electrons can flow across the interface, resulting in a transient current in the external load.[5,6] Therefore, the magnitude of the negative piezopotential at the top of the NW would govern the measured output voltage *via* the external load. Comparing the semiquantitatively calculated potential (Figure 5) and the measured output voltage (Figure 3), the calculated potential of −298 mV (as shown in Figure 5f) corresponds to the measured voltage of around −160 mV (as shown in Figure 3b), showing a reasonable agreement.

For an AFM tip pushing along $\pm y$-axis directions (Figure 4c,d), Figure 5b,c (side view) and 5g,h (top view) exhibit the calculated piezopotential distributions in the bent NW without slipping between an AFM tip and the NW. Regarding pushing along $+y$-axis direction, the NW would be applied by not only a partial force $f \cdot \cos\theta$ for bending but also a significant force $f \cdot \sin\theta$ for pulling along $+c$-axis direction (Figure 4c), leading to the positive piezopotential (1.848 to 1.289 V) at the whole top of the NW,[7,8] as shown in Figure 5g. The positive piezopotential would set the Schottky barrier (at the interface between the Pt/ZnO) to reversed bias, probably causing no current flow across the Schottky interface or even the observed positive voltage peaks through overcoming the reversely biased Schottky barrier. However, the above expected result is inconsistent with the experimental observation in Figure 3c. Concerning the pushing of $+y$-axis direction without slipping between an AFM tip and the NW (Figure 4d), in addition to the bending force $f \cdot \cos\theta$, the inclined NW would be pressed by a force $f \cdot \sin\theta$ along $-c$-axis direction, resulting in the negative piezopotential

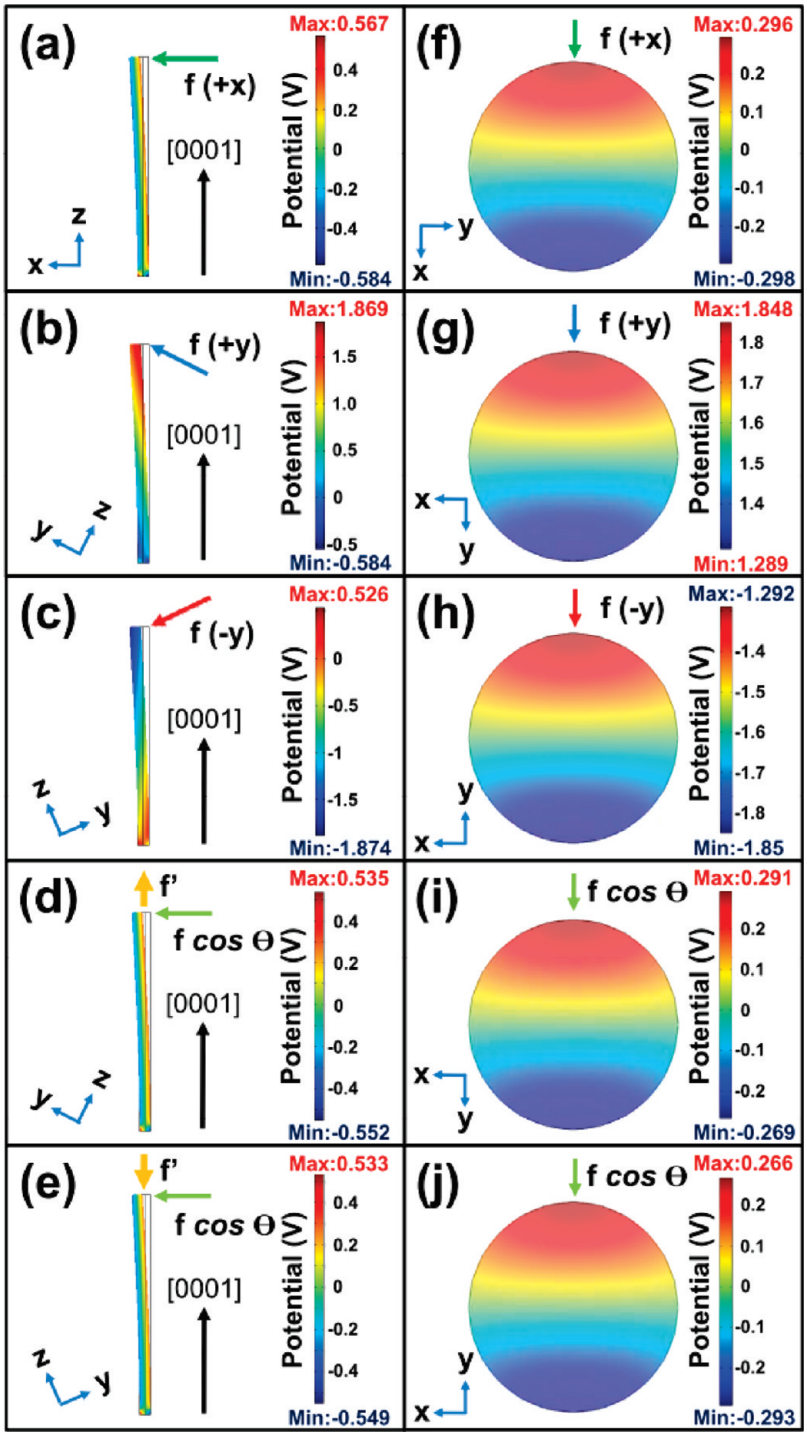

Figure 5. Calculated piezoelectric potential distribution for a ZnO NW. The dimension of the NW is radius a = 25 nm, length l = 1000 nm, and the external forces are f = 80 nN, $f' = 1/128\, f \cdot \sin\theta$. (a−e) and (f−j) are side and top views (at z_0 = 995 nm) of the output of the piezoelectric potential in the NW, respectively.

(−1.292 to −1.85 V) at the entire top of the NW (Figure 5h), which is higher than the calculated one along +x-axis direction (−0.298 V) (Figure 5f), not in agreement with our experimental results (Figure 3b,d). Therefore, the inconsistency is most likely due to the fact that there is a slip between the AFM tip and the NW during scanning. However, if we assume that there is no any tangential force between an AFM tip and the NW, that is, perfectly slipping between a tip and the NW (without any partial force along c-axis), the NW would be only applied by a partial force $f \cdot \cos\theta$ for bending under an AFM tip pushing along ±y-axis directions (Figure 4c,d), which should result in equal output voltages with the tip scanning along ±y-axis directions. Hence, it is not reasonable if we assume a perfect slip without friction.

With a small tangential force ($f' = 1/128\ f \cdot \sin\theta$) between an AFM tip and the NW, the calculated piezopotential distributions in the bent NW by the tip pushing along $\pm y$-axis directions are shown in Figure 5d,e (side view) and 5i,j (top view). The correction factor, 1/128, is used to take account of a slip between the AFM tip and the NW during scanning. For pushing along $+y$-axis direction, the calculated potential of -269 mV (as shown in Figure 5i) corresponds to the measured voltage of around -130 mV (as shown in Figure 3c). For pushing along $-y$-axis direction, the calculated potential of -293 mV (as shown in Figure 5j) corresponds to the measured voltage of around -150 mV (as shown in Figure 3d). Compared to the calculated potential of -298 mV (corresponding to the measured voltage of around -160 mV) for pushing along $+x$-axis direction, the above-mentioned calculated results more closely approach the real experimental results. Furthermore, the anisotropic electricity generation along $\pm y$-axis directions can be understood due to the piezopotentials originating from the small tangential force between a tip and the NW. In addition, the measured output voltages along $\pm x$-axis directions are higher than these along $\pm y$-axis directions, which is likely due to the difference in the effective forces for bending the NW in the two cases.

CONCLUSIONS

The anisotropic electricity generation has been statistically demonstrated and analyzed with the oblique-aligned ZnO NWAs synthesized by combing the technique of the OAD for preparing the seed layer and the hydrothermal method for NW growth. Through reducing in-plane symmetry in the NWAs, the output of the NG depends on the direction along which the tip of the AFM scans. To understand the mechanism of the anisotropic output, the calculated piezopotential distributions in a bent ZnO NW have been semiquantitatively analyzed under an external force with the four different directions in reference to the inclining direction of the NWs. Because the highly conductive AZO buffer layer was utilized as the bottom electric contact instead of the intrinsic ZnO layer, the oblique-aligned ZnO NWAs show excellent performance as piezoelectric NGs. Our study provides comprehensive experimental and theoretical base for optimizing the performance of NGs.

EXPERIMENTAL SECTION

Synthesis of Oblique-Aligned ZnO NWAs. The oblique-aligned ZnO NWAs were grown on Si(100) substrate with a sputtering process and a subsequent hydrothermal method. Pure ZnO target (99.99%) and pure Al target (99.99%) were utilized as the sputtering source. First, an Al-doped ZnO (AZO) buffer layer was prepared by the co-sputtering process using ZnO/Al targets under a 1 rpm rotating substrate in argon at 460 °C for 2 h at the oblique angle of 30° with respect to the surface normal of the sputtering targets. Second, the ZnO bent columnar seed was deposited by pure ZnO sputtering in a reduced atmosphere with 20% hydrogen/argon mixture gas at 280 ± 1 °C for 2 h at the oblique angle of 30° without the substrate rotation. For the final hydrothermal process, the oblique-aligned ZnO NWAs were synthesized in a solution mixed by 0.005 M zinc acetate dehydrate ($Zn(Ch_3COO)_2 \cdot 2H_2O$) and 0.005 M hexamethylenetetramine (HMT $C_6H_{12}N_4$) at the ratio of 1:1, heated at 80 ± 1 °C for 6 h. More details of oblique-aligned NWA synthesis are described elsewhere.[29]

Morphology and Structure Characterization. The morphological studies of our samples were performed with a JEOL JSM-6500 field emission SEM and a JEOL 3000F field emission TEM.

Piezoelectric Measurements of Oblique-Aligned NWAs. Piezoelectric measurements were performed using AFM (Molecular Force Probe MFP-3D from Asylum Research) with a conducting Pt-coated Si tip, which has a cone angle of 70°. The ZnO NWA samples were fixed on a piece of metal plate with Ag pastes, with the AZO buffer layer deposited at the bottom as a common grounded electrode. The rectangular cantilever of the AFM had a spring constant of 1.55 N/m. A constant normal force of 5 nN was maintained between the tip and NW arrays in the contact mode. The output voltage across an outside load of resistance R_L of 500 MΩ was continuously monitored as the tip scanned over the NWs. No external voltage was applied during the experiment measurement.

Acknowledgment. This work was supported by DARPA (HR0011-09-C-0142, Program manager, Dr. Daniel Wattendorf), BES DOE (DE-FG02-07ER46394), and National Science Council of Taiwan (99-2112-M-002-024-MY3 and 100-2917-I-002-009).

Note Added after ASAP Publication: This paper was originally published on July 20, 2011. Subsequently, the affiliations for Jun-Han Huang and Chuan-Pu Liu were revised and the corrected version was reposted on August 1, 2011.

REFERENCES AND NOTES

1. Special Issue on Sustainability and Energy. *Science* **2007**, *315*, 721−896.
2. Special Issue on Harnessing Materials for Energy. *MRS Bull.* **2008**, *33*, No. 4.
3. Wang, Z. L. Towards Self-Powered Nanosystems: From Nanogenerators to Nanopiezotronics. *Adv. Funct. Mater.* **2008**, *18*, 3553–3567.
4. Wang, Z. L. ZnO Nanowire and Nanobelt Platform for Nanotechnology. *Mater. Sci. Eng. R* **2009**, *64*, 33–71.
5. Wang, Z. L.; Song, J. H. Piezoelectric Nanogenerators Based on Zinc Oxide Nanowire Arrays. *Science* **2006**, *312*, 242–246.
6. Lu, M. P.; Song, J.; Lu, M. Y.; Chen, M. T.; Gao, Y.; Chen, L. J.; Wang, Z. L. Piezoelectric Nanogenerator Using p-Type ZnO Nanowire Arrays. *Nano Lett.* **2009**, *9*, 1223–1227.
7. Yang, R.; Qin, Y.; Dai, L.; Wang, Z. L. Power Generation with Laterally-Packaged Piezoelectric Fine Wires. *Nat. Nanotechnol.* **2009**, *4*, 34–39.
8. Cha, S. N.; Seo, J. S.; Kim, S. M.; Kim, H. J.; Park, Y. J.; Kim, S. W.; Kim, J. M. Sound-Driven Piezoelectric Nanowire-Based Nanogenerators. *Adv. Mater.* **2010**, *22*, 4726–4730.
9. Xi, Y.; Song, J.; Xu, S.; Yang, R.; Gao, Z.; Hu, C.; Wang, Z. L. Growth of ZnO Nanotube Arrays and Nanotube Based Piezoelectric Nanogenerator. *J. Mater. Chem.* **2009**, *19*, 9260–9264.
10. Lin, Y. F.; Song, J. H.; Ding, Y.; Liu, S. Y.; Wang, Z. L. Piezoelectric Nanogenerator Using CdS Nanowires. *Appl. Phys. Lett.* **2008**, *92*, 022105.
11. Lu, M. Y.; Song, J. H.; Lu, M. P.; Lee, C. Y.; Chen, L. J.; Wang, Z. L. ZnO−ZnS Heterojunction and ZnS Nanowire Arrays for Electricity Generation. *ACS Nano* **2009**, *3*, 357–362.
12. Chen, X.; Xu, S.; Yao, N.; Shi, Y. 1.6 V Nanogenerator for Mechanical Energy Harvesting Using PZT Nanofibers. *Nano Lett.* **2010**, *10*, 2133–2137.

13. Qi, Y.; Kim, J.; Nguyen, T. D.; Lisko, B.; Purohit, P. K.; McAlpine, M. C. Enhanced Piezoelectricity and Stretchability in Energy Harvesting Devices Fabricated from Buckled PZT Ribbons. *Nano Lett.* **2011**, *11*, 1331–1336.
14. Park, K. I.; Xu, S.; Liu, Y.; Hwang, G. T.; Kang, S. J. L.; Wang, Z. L.; Lee, K. J. Piezoelectric $BaTiO_3$ Thin Film Nanogenerator on Plastic Substrates. *Nano Lett.* **2010**, *10*, 4939–4943.
15. Chang, C.; Tran, V. H.; Wang, J.; Fuh, Y. K.; Lin, L. Direct-Write Piezoelectric Polymeric Nanogenerator with High Energy Conversion Efficiency. *Nano Lett.* **2010**, *10*, 726–731.
16. Huang, C. T.; Song, J.; Tsai, C. M.; Lee, W. F.; Lien, D. H.; Gao, Z.; Hao, Y.; Chen, L. J.; Wang, Z. L. Single-InN-Nanowire Nanogenerator with up to 1 V Output Voltage. *Adv. Mater.* **2010**, *22*, 4008–4013.
17. Wang, X.; Song, J.; Zhang, F.; He, C.; Hu, Z.; Wang, Z. L. Electricity Generation Based on One-Dimensional Group-III Nitride Nanomaterials. *Adv. Mater.* **2010**, *22*, 2155–2158.
18. Su, W. S.; Chen, Y. F.; Hsiao, C. L.; Tu, L. W. Generation of Electricity in GaN Nanorods Induced by Piezoelectric Effect. *Appl. Phys. Lett.* **2007**, *90*, 063110.
19. Huang, C. T.; Song, J.; Lee, W. F.; Ding, Y.; Gao, Z.; Hao, Y.; Chen, L. J.; Wang, Z. L. GaN Nanowire Arrays for High-Output Nanogenerators. *J. Am. Chem. Soc.* **2010**, *132*, 4766–4771.
20. Zhou, J.; Xu, N. S.; Wang, Z. L. Dissolving Behavior and Stability of ZnO Wires in Biofluids: A Study on Biodegradability and Biocompatibility of ZnO Nanostructures. *Adv. Mater.* **2006**, *18*, 2432–2435.
21. Chen, M. T.; Lu, M. P.; Wu, Y. J.; Song, J.; Lee, C. Y.; Lu, M. Y.; Chang, Y. C.; Chou, L. J.; Wang, Z. L.; Chen, L. J. Near UV LEDs Made with *In Situ* Doped p−n Homojunction ZnO Nanowire Arrays. *Nano Lett.* **2010**, *10*, 4387–4393.
22. Xu, S.; Xu, C.; Liu, Y.; Hu, Y.; Yang, R.; Yang, Q.; Ryou, J. H.; Kim, H. J.; Lochner, Z.; Choi, S.; Dupuis, R.; Wang, Z. L. Ordered Nanowire Array Blue/Near-UV Light Emitting Diodes. *Adv. Mater.* **2010**, *22*, 4749–4753.
23. He, J. H.; Chang, P. H.; Chen, C. Y.; Tsai, K. D. Electrical and Optoelectronic Characterization of ZnO Nanowire Contacted by Focused-Ion-Beam-Deposited Pt. *Nanotechnology* **2009**, *20*, 135701.
24. He, J. H.; Ho, C. H.; Chen, C. Y. Polymer Functionalized ZnO Nanobelt as Gas Sensor with a Significant Response Enhancement. *Nanotechnology* **2009**, *20*, 065503.
25. Yang, Q.; Guo, X.; Wang, W.; Zhang, Y.; Xu, S.; Lien, D. H.; Wang, Z. L. Enhancing Sensitivity of a Single ZnO Micro-/Nanowire Photodetector by Piezo-phototronic Effect. *ACS Nano* **2010**, *4*, 6285–6291.
26. Chen, M. W.; Chen, C. Y.; Lien, D. H.; Ding., Y.; He, J. H. Photoconductive Enhancement of Single ZnO Nanowire through Localized Schottky Effects. *Opt. Express* **2010**, *18*, 14837.
27. Hu, Y.; Zhou, J.; Yeh, P. H.; Li, Z.; Wei, T. Y.; Wang, Z. L. Supersensitive, Fast-Response Nanowire Sensors by Using Schottky Contacts. *Adv. Mater.* **2010**, *22*, 3327–3332.
28. Chen, P. C.; Shen, G.; Zhou, C. Chemical Sensors and Electronic Noses Based on 1-D Metal Oxide Nanostructures. *IEEE Trans. Nanotechnol.* **2008**, *7*, 668–682.
29. Huang, J. H.; Chen, C. Y.; Lai, Y. F.; Shih, Y. I; Lin, Y. C.; He, J. H.; Liu, C. P. Large-Area Oblique-Aligned ZnO Nanowires through a Continuously Bent Columnar Buffer: Growth, Microstructure, and Antireflection. *Cryst. Growth Des.* **2010**, *10*, 3297–3301.
30. Wang, Z. L. Energy Harvesting Using Piezoelectric Nanowires—A Correspondence on "Energy Harvesting Using Nanowires?" by Alexe *et al*. *Adv. Mater.* **2009**, *21*, 1311–1315.
31. Gao, Y.; Wang, Z. L. Equilibrium Potential of Free Charge Carriers in a Bent Piezoelectric Semiconductive Nanowire. *Nano Lett.* **2009**, *9*, 1103–1110.
32. Riaz, M.; Song, J.; Nur, O.; Wang, Z. L.; Willander, M. Study of the Piezoelectric Power Generation of ZnO Nanowire Arrays Grown by Different Methods. *Adv. Funct. Mater.* **2011**, *21*, 628–633.
33. Mantini, G.; Gao, Y.; D'Amico, A.; Falconi, C.; Wang, Z. L. Equilibrium Piezoelectric Potential Distribution in a Deformed ZnO Nanowire. *Nano Res.* **2009**, *2*, 624–629.
34. Hu, Y.; Zhang, Y.; Xu, C.; Zhu, G.; Wang, Z. L. High-Output Nanogenerator by Rational Unipolar Assembly of Conical Nanowires and Its Application for Driving a Small Liquid Crystal Display. *Nano Lett.* **2010**, *10*, 5025–5031.